The Journal of Immunology

# Mettl3 Deficiency Sustains Long-Chain Fatty Acid Absorption through Suppressing Traf6-Dependent Inflammation Response

Xin Zong, Jing Zhao, Hong Wang, Zeqing Lu, Fengqin Wang, Huahua Du and Yizhen Wang



*J Immunol* 2019; 202:567-578; Prepublished online 19 December 2018;
doi: 10.4049/jimmunol.1801151
http://www.jimmunol.org/content/202/2/567



*The Journal of Immunology* is published twice each month by
The American Association of Immunologists, Inc.,
1451 Rockville Pike, Suite 650, Rockville, MD 20852

Print ISSN: 0022-1767 Online ISSN: 1550-6606.

# Mettl3 Deficiency Sustains Long-Chain Fatty Acid Absorption through Suppressing Traf6-Dependent Inflammation Response

**Xin Zong,* Jing Zhao,* Hong Wang,* Zeqing Lu,*,† Fengqin Wang,*,† Huahua Du,*,† and Yizhen Wang*,†**

**A better understanding of the molecular mechanism of intestinal fatty acid absorption could lead to novel approaches to treatment and prevention of fatty acid–related metabolic diseases. Although it is confirmed that absorption of long-chain fatty acids (LCFAs) decreases during the pathological processes, the genetic basis and molecular mechanisms remain largely unknown. $N^6$-methyladenosine ($m^6A$) is the most prevalent internal modification on eukaryotic mRNA. Recently, $m^6A$ has been found to play important roles in inflammation and antiviral responses. In this study, we show that deficiency of Mettl3, the core methyltransferase of $m^6A$, exerts antimalabsorption of LCFA activity in vitro through inhibiting the inflammation response mediated by LPS. To substantiate this finding further, we found the levels of triglycerides were also sustained in cells with depleted Mettl3, which were cultured in Transwell to polarize with villus formation to simulate the situation in vivo. Mechanistically, depletion of Mettl3 decreases the $m^6A$ level of Traf6 mRNA, thereby its transcripts are entrapped in the nucleus, followed by the decreased expression of Traf6, leading to the suppression of NF-κB and MAPK signaling pathway. Thus, the inflammation response was suppressed, resulting in the sustained absorption of LCFA. Moreover, we found that ectopic expression of Traf6 largely abolishes the sustained absorption LCFA in Mettl3 depletion cells. Collectively, silencing Mettl3 could sustain LCFA absorption through blocking the TRAF6-dependent inflammation response. Our work uncovers a critical function of $m^6A$ methylation and provides insight into critical roles of Mettl3 in LCFA absorption and inflammatory disease.** *The Journal of Immunology*, **2019, 202: 567–578.**

Long-chain fatty acids (LCFAs) are particularly needed during periods of growth and development and serve several important functions in the human body (1). First, LCFAs are a major component of fat, which is one of the most important sources of energy, supplying 9 kcal/g, about as twice as much of that contributed by either protein or carbohydrate, each at 4 kcal/g (2). In addition, dietary LCFA provides the essential fatty acids and represents the only source of precursors of eicosanoids such as prostanoids, thromboxanes, leukotrienes, and lipoxins (3). Fatty acids are taken up by membrane-associated fatty acid–binding proteins—that is, fatty acid transporters on the apical membrane of enterocyte (4), including cluster determinant 36 (CD36), plasma membrane–associated fatty acid–binding protein (Fabp), and a family of fatty acid transport proteins (Fatp) 1–6 (5–7). After entering the enterocytes, monoacylglycerols and fatty acids are largely reconstituted to form triglycerides and are then incorporated into chylomicrons. Fatty acid compositions of triglycerides in intestinal lipoproteins reflect the fatty acids absorption (8, 9). Following secretion into intestinal lymph, chylomicrons enter the blood through the thoracic duct.

Because intestinal fatty acid absorption is a multistep process, many factors that modulate the transport of fatty acids from the intestinal lumen to the lymph may influence the efficiency of the absorption. For example, the intestinal capacity to absorb LCFAs is severely reduced in rats with methotrexate-induced mucositis (10). Intestinal secretion induced by cholera toxin may delay the mucosal uptake and lymphatic transport of LCFAs, whereas triglyceride formation maybe not affected in the epithelial cells (11). Endotoxins induce severe anorexia and liver lipid accumulation during sepsis through hepatocyte autophagy-maintained lipid metabolism homeostasis (12). The persistent IL-22 production from group 3 innate lymphoid cells results in impaired host lipid metabolism by decreasing lipid transporter expression in the small bowel (13). The field's accumulative data increasingly revealed LCFA absorption-modulated factors, yet the genetic basis and the mechanisms of malabsorption of LCFA during the pathological processes remain largely unknown. So far, it has only been found that the pathological factors impair the uptake and transport of LCFAs through decreasing the expression of fatty acid metabolism-related genes, especially CD36 and Fatp4 (10, 11, 14, 15). However, CD36 also plays a role as a TLR-dependent signaling receptor, initiating a downstream cascade upon ligand

*College of Animal Sciences, Zhejiang University, Hangzhou, Zhejiang Province 310058, People's Republic of China; and †Key Laboratory of Animal Nutrition and Feed Science in Eastern China, Ministry of Agriculture, Hangzhou, Zhejiang Province 310058, People's Republic of China

Received for publication August 21, 2018. Accepted for publication November 13, 2018.

This work was supported by a grant from the National Natural Science Foundation of China (3163000269, awarded to Y.W.), a grant from the National Natural Science Foundation of China (31601947, awarded to Z.L.), and a grant from the Modern Agroindustry Technology Research System (CARS-36, awarded to Y.W.).

Address correspondence and reprint requests to Prof. Yizhen Wang, Zhejiang University, 866 Yuhangtang Road, Hangzhou, Zhejiang Province 310058, People's Republic of China. E-mail address: yzwang321@zju.edu.cn

The online version of this article contains supplemental material.

Abbreviations used in this article: Bodipy FA, BODIPY FL C16; CD36, cluster determinant 36; Fabp, plasma membrane–associated fatty acid–binding protein; Fatp, fatty acid transport protein; FISH, fluorescence in situ hybridization; Fwd, forward; GC/MS, gas chromatography/mass spectrometry; IB, immunoblot analysis; IF, immunofluorescence; IP, immunoprecipitation; IPEC-J2, intestinal porcine epithelial cell line J2; LCFA, long-chain fatty acid; $m^6A$, $N^6$-methyladenosine; q-PCR, quantitative real-time PCR; Rev, reverese; sh, short hairpin; shRNA, short hairpin RNA.

binding (16). Similarly, Baranova et al. (17) reported that CD36 could act as a phagocytic receptor to mediate JNK pathway signaling induced by Gram-negative bacteria and LPS. Hoebe et al. (18) reported CD36 mutation partially blocked activation of MAPK and IκB degradation, which were necessary for inflammation response. Conversely, Cifarelli et al. (19) found depletion of CD36 induced neutrophil infiltration and inflammation in intestine. Taking these findings together, the relationship between inflammation and fatty acids absorption has been a controversial issue.

$N^6$-methyladenosine ($m^6A$) is the most prevalent internal modification on eukaryotic mRNA (20). The level of $m^6A$ is maintained in dynamic balance through methyltransferases (Mettl3 and Mettl14) and demethylases (Fto and Alkbh5) (21–24). The fundamental cellular functions of $m^6A$ have been connected directly to the splicing, translation, and stability of mRNA and involved in adipogenesis, cancer, stem cells, and circadian clock (25–28). More recently, $m^6A$ has been shown to play important roles in innate immunity. For example, $m^6A$ could affect the LPS-induced inflammatory response in human dental pulp cells by regulating the alternative splicing of MyD88 (29); Alkbh5 could inhibit antiviral innate responses by entrapping selected antiviral transcripts in the nucleus by erasing their $m^6A$ modification (30). However, the role of $m^6A$ modification in inflammation response, especially in the malabsorption induced by inflammation, is unknown.

Based on this evidence, we hypothesized that $m^6A$ modification plays a critical role in inflammation-induced malabsorption of LCFA. To address the hypothesis, intestinal epithelial cells with depleted Mettl3 and a LPS-triggered inflammation response–induced LCFA malabsorption model were established. Our work suggests that Mettl3 might show considerable potential as a new target for the development of therapies directed against fatty acids malabsorption and inflammatory disease.

## Materials and Methods

### *Cell culture and LPS stimulation*

Intestinal porcine epithelial cell line J2 (IPEC-J2) cells were purchased from the Cell Bank of the Chinese Academy of Sciences (Shanghai, People's Republic of China) and were cultured as described previously (31). All cells tested negative for mycoplasma contamination. The cells were cultured in six-well culture dishes until they reached ∼80% confluence and were then treated with 10 μg/ml *Escherichia coli* strain O111:B4 LPS (Sigma-Aldrich, St. Louis, MO) for various times. Cells without LPS stimulation were used as controls.

### *Reagents*

Abs to the following were used for immunoprecipitation (IP), immunoblot analysis (IB), and immunofluorescence (IF): β-actin (1:1000 for IB; Sungene Biotech); TRAF6 (1:500 for IB), FTO (1:1000 for IB), and ALKBH5 (1:1000 for IB), all from Abcam; HRP-coupled secondary Ab (1:1000 for IB), phospho-IKKα/β (1:1000 for IB), p65 (1:1000 for IB), phospho-p65 (1:1000 for IB), phospho-IκBα (1:1000 for IB), and IκBα (1:1000 for IB), all from Cell Signaling Technology; METTL3 (1:1000 for IB; Proteintech); Mettl14 (1:1000 for IB; Sigma-Aldrich); ERK (1:1000 for IB), phospho-ERK (1:1000 for IB), JNK (1:1000 for IB), phospho-JNK (1:1000 for IB), p38 (1:1000 for IB), IKKα (1:1000 for IB), IKKβ (1:1000 for IB), from HuaAn Biotechnology; phospho-p38 (1:1000 for IB; Multi Sciences); DAPI (62247, 1:1000 for IF), Alexa Fluor 488 (1:500 for IF), and Alexa Fluor 546 (1:500 for IF), all from Thermo Fisher Scientific; and Ab specific to $m^6A$ (1:200 for IP) from Synaptic Systems.

### *Molecular cloning of related genes*

The Mettl3 and Traf6 full-length coding sequences were obtained from IPEC-J2 cells by RT-PCR and were subsequently cloned into pcDNA3.1-vectors. Each construct was confirmed by sequencing. The corresponding primers used in this study are as follows: BamHI-Mettl3-forward (Fwd): 5′-GTTGGATCCGCCACCATGTCGGACACGTGGAGCTC-3′; ECORI-Mettl3-reverse (Rev): 5′-CCCGAATTCTCACTTATCGTCGTCATCCTTGTAATC TAAATTCTTAGGTTT-3′; NheI-Traf6-Fwd: 5′-GTTGCTAGCGCCACCATGAGTCTGCTACATTGTGA-3′; KpnI-Traf6-Rev: 5′-CCCGGTACCTCACTTATCGTCGTCATCCTTGTAATCTCATGTCCCCGAGTCTGTA-3′.

### *Lentiviral short hairpin RNAs*

Lentiviral short hairpin (sh) RNAs (shRNAs) were performed as described previously (32). shRNA targeting sequences are listed below: Mettl3-1: 5′-TTCCGCTGAGCCACGATATAA-3′; Mettl3-2: 5′-CAGAAATGCAGTATGATATAT-3′; scramble control sequence: 5′-AACAGTCGCGTTTGCGACTGG-3′.

All the shRNA targeting sequences were cloned into DECIPHER pRSI9-U6-(sh)-UbiC-TagRFP-2A-Puro (obtained from Qian' laboratory, Cornell University). Lentiviral particles were packaged using Lenti-X 293T cells (obtained from Qian' laboratory, Cornell University). Virus-containing supernatants were collected at 48 h after transfection and filtered to eliminate cells. IPEC-J2 cells were infected by the lentivirus for 48 h before selection by 3 μg/ml puromycin.

### *Immunoblot analysis*

Cells were lysed on ice in SDS-PAGE sample buffer (50 mM Tris [pH 6.8], 100 mM DTT, 2% SDS, 0.1% bromophenol blue, 10% glycerol), followed by heating for 10 min. Proteins were separated by 10% SDS-PAGE and electrophoretically transferred onto a polyvinylidene fluoride membrane (MilliporeSigma, Billerica, MA). The membranes were blocked in TBS (50 mM Tris, pH 7.5, 150 mM NaCl, 1 mM EDTA) containing 5% nonfat milk and 0.1% Tween 20 at room temperature for 1 h and then incubated with the primary Abs overnight at 4°C. After washing with TBST, proteins were detected with HRP-conjugated secondary Abs at room temperature for 1 h. Specific bands were visualized with an ECL detection kit (Biosharp, Hefei, China) and scanned using a ChemiScope series 3400 mini system (Clinx Science Instruments, Shanghai, China). Band densities were quantified and normalized to β-actin using Image J v1.47 software (National Institutes of Health, Bethesda, MD).

### *Quantitative real-time PCR*

Total RNA was isolated using TRIzol reagent (Invitrogen). For cDNA synthesis, 2 μg of RNA from each sample was reverse transcribed using M-MLV Reverse Transcriptase (Thermo Fisher Scientific). Subsequently, quantitative real-time PCR (q-PCR) was conducted in triplicate on a StepOne Real-Time PCR System (ABI StepOnePlus; Applied Biosystems, Foster City, CA) using FastStart Universal SYBR Green Master (ROX) (Roche). The $2^{-\Delta\Delta}$ cycle threshold method was used to determine the mRNA expression levels. Primers for amplifying each target are listed below: Npc1l1-Fwd: 5′-TCAGGAACGCACACTCTGAC-3′; Npc1l1-Rev: 5′-AAGTGTCAGTGAGCAGACGG-3′. Fatp4-Fwd: 5′-ACCAGAGTGGCTGTCGTTC-3′; Fatp4-Rev: 5′-CTGCACAGGAAGGTCAGGTTA-3′. Abcg5-Fwd: 5′-CGGCTCGAGGCTATTTTACATTC-3′; Abcg5-Rev: 5′-GCTGCAAGTGAAATTCTGTCCA-3′. Lfabp-Fwd: 5′-GGGAGTAGCCTCATTGCCAC-3′; Lfabp-Rev: 5′-ATGAGTTCATCGGGCAGACC-3′. Caveolin-Fwd: 5′-GGGGCAAATACGTAGACTCGG-3′; Caveolin-Rev: 5′-TGGGCTTGTAGATGTTGCCC-3′. Cd36-Fwd: 5′-TGGTTTAGGAATCCCACTGCC-3′; Cd36-Rev: 5′-CGCCCCACCTCCAAGTATC-3′. Abca1-Fwd: 5′-AAGAAGATGCTGCCAGTGTGT-3′; Abca1-Rev: 5′-CTGAAGGATGTCCGCGGTG-3′. Srebp-1c-Fwd: 5′-CTTCCACCATGAGCTCCCC-3′; Srebp-1c-Rev: 5′-CACCGACGGGTACATCTTCA-3′. Mtp-Fwd: 5′-TCAGGTGGTCATTGAAGCCC-3′; Mtp-Rev: 5′-GGTGACAAGCCAGCATAGGA-3′. Il6-Fwd: 5′-TGGCTACTGCCTTCCCTACC-3′; Il6-Rev: 5′-CAGAGATTTTGCCGAGGATG-3′. Tnfα-Fwd: 5′-CGACTCAGTGCCGAGATCAA-3′; Tnfα-Rev: 5′-CCTGCCCAGATTCAGCAAAG-3′. Il1β-Fwd: 5′-TGATTGTGGCAAAGGAGGA-3′; Il1β-Rev: 5′-TTGGGTCATCATCACAGACG-3′. Mettl3-Fwd: 5′-CCACTTCTGGTGGCCCTAAG-3′; Mettl3-Rev: 5′-CGCCAGATCAGAAAGGTGGT-3′. Mettl14-Fwd: 5′-GAGATTGCAGCTCCTCGATCA-3′; Mettl14-Rev: 5′-CCCCACTTGCGTAAACACAC-3′. Fto-Fwd: 5′-GCATGGCTGCTTATTTCGGG-3′; Fto-Rev: 5′-TGCATCAGAGCCCTTCACTG-3′. Alkbh5-Fwd: 5′-CCAGTTCAAGCCTATCCGGG-3′; Alkbh5-Rev: 5′-ATCCACTGAGCACAGTCACG-3′. β-actin-Fwd: 5′-TGGCGCCCAGCACGATGAAG-3′; β-actin-Rev: 5′-GATGGAGGGGCCGGACTCGT-3′.

### *$m^6A$ dot blot*

mRNA was purified from total RNA using Dynabeads Oligo(dT)25 (Thermo Fisher Scientific). Equal amounts of mRNA were spotted to a Amersham Hybond-N+ membrane (GE Healthcare), followed by UV crosslinking at UV 254 nm, 0.12 J/cm$^2$. After blocking in PBS with Tween 20 containing 5% nonfat milk and 0.1% Tween 20 for 1 h, the membrane was incubated with 1:1000 diluted anti-$m^6A$ Ab overnight at 4°C. The membrane was incubated with secondary Ab for 1 h. The dots were visualized by ECL

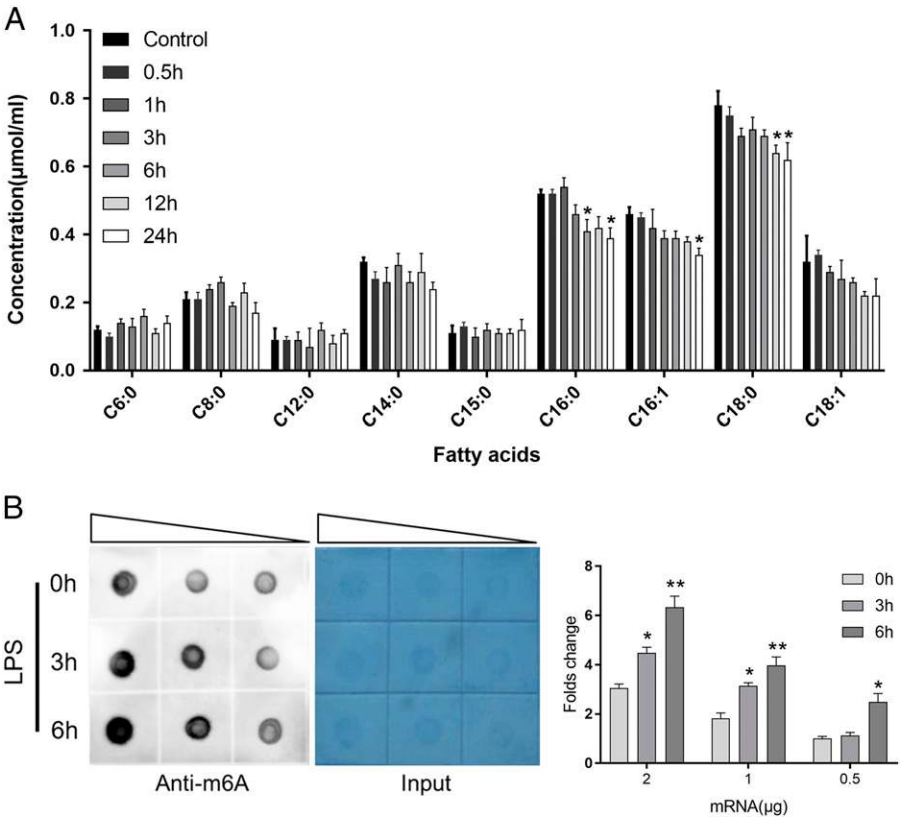


**FIGURE 1.** Inhibition effect of LPS on LCFA absorption in IPEC-J2 cells was related to $m^6A$ methylation. IPEC-J2 cells were treated with 10 μg/ml LPS for various times, and cells without LPS stimulation were used as controls. (**A**) The composition of fatty acids in whole lysate measured by GC/MS. (**B**) $m^6A$ dot blot to measure the $m^6A$ levels with purified mRNA from total RNA. Methylene blue staining was used for loading control. The right panel shows the relative levels quantified by densitometry and normalized to control. The data are expressed as the mean ± SEM. Statistically significant difference relative to the control (0 h) ($n$ = 3, biological replicates). $^*p < 0.05$.

detection kit and scanned using a ChemiScope series 3400 mini system. Methylene blue staining was used to show the amount of total RNA on the membrane.

### *Gas chromatography/mass spectrometry*

To examine compositional differences in individual lipid species, gas chromatography/mass spectrometry (GC/MS) method was used. Peaks of the fatty acid were identified, and the quantity of the individual fatty acid species were calculated from a standard curve of five dilutions of the standards in an analogous matter as for the HPLC-based analyses. The procedures closely followed those of Chen et al. (33).

### *Bodipy-labeled fatty acid uptake assay*

Fatty acid uptake was measured using the fluorescent-labeled LCFA, 4,4-difluoro-5,7-dimethyl-4-bora-3a, and 4a-diaza-s-indacene-3-hexadecanoic acid (BODIPY FL C16; hereafter referred to as Bodipy FA; Invitrogen). The cells were serum-starved with FBS-free DMEM F12 medium (Life Technologies) for at least 8 h. The cells were then treated with 10 μg/ml LPS for 0, 3, or 6 h and briefly washed with PBS. Then, Bodipy FA, preincubated with fatty acid-free BSA (2:1 M ratio) in PBS for 10 min in a 37°C water bath, was added to the cells for 5 min at 37°C. For cells in 96-well plates, assays were conducted in the presence of the quenching agent trypan blue, and intracellular fluorescence was measured immediately (bottom read) with a microplate reader (excitation 488 nm, emission 515 nm, cut-off 495 nm, SpectraMax M5; Molecular Probes). Bodipy signals were normalized to cell number measured with resazurin (no. R7017; Sigma-Aldrich) (34). For confocal microscopy observation, cells were grown on coverslips and visualized using a Zeiss LSM710 confocal microscope. For flow cytometry analysis, cells were plated on six-well plates and collected by trypsinization, transferred into the respective FACS tube (Becton Dickinson), and resuspended with PBS. Each FACS tube was vortexed before being analyzed by flow cytometer (BD Biosciences, San Diego, CA).

### *Scanning electron microscopy and triglyceride measurement*

Cells were counted and seeded ($5 \times 10^4$ cells per well) on a 0.4-μm Transwell (Corning). Confluent and polarized 21-d cultured IPEC-J2 cells were employed with a transmembrane electrical resistance of >300 (35), followed by 10 μg/ml LPS treatment for 0, 6, or 12 h. For scanning electron microscopy, cells were fixed with 2.5% (w/v) glutaraldehyde at 4°C overnight, followed by washing with PBS twice. Cells were harvested and postfixed with 1% osmium tetroxide for 1 h, then dehydrated for 15 min in each of a graded ethanol series (50, 70, 80, 90, 95, and 100%). They were then transferred to absolute acetone for 20 min, a mixture (v/v = 1:1) of alcohol and iso-amyl acetate for 30 min, then pure iso-amyl acetate for 1 h. Finally, specimens were dehydrated in a Hitachi Model HCP-2 critical point dryer with liquid $CO_2$. The dehydrated specimens were coated with gold-palladium and observed in a Philips Model XL30 ESEM. For triglyceride measurement, cells were harvested and measured using a Triglyceride Reagent Set (Pointe Scientific) according to the manufacturer's instructions.

### *Cytokine assay and ELISA*

Concentrations of TNF-α, IL-6, and IL-1β in cell culture supernatants obtained from different groups were determined using commercial ELISA quantitative kits (RayBiotech, Norcross, GA) according to the manufacturer's instructions.

### *RNA interference*

Small-interfering RNAs that target pig Alkbh5 (no. 1: 5′-CGTCCCGGGACAACTACAA-3′; no, 2: 5′-AGGACGAGTGCGCCAAGAT-3′; no, 3: 5′-CCGTCATCAACGACTACCA-3′) were designed and synthesized by RiboBio. Cells cultured in six-well plates at a density of $1.8 \times 10^6$ cells per well were transfected with siRNA (final concentration, 20 nM) using Lipofectamine 2000 (Invitrogen), according to the manufacturer's instructions. At 24 h after transfections, the cells were treated with LPS at the indicated time.

### *RNA fractionation, RNA extraction, and RT-PCR*

Nucleocytoplasmic fractionations of RNA were performed as described previously (36). Briefly, after LPS treatment, cell pellets from a 80% confluent 10-cm plate were collected and lysed in lysis buffer (10 mM Tris-HCl, 140 mM NaCl, 1.5 mM MgCl2, 10 mM EDTA, 0.5% Nonidet P-40 and 40 U/ml RNasin, pH 7.4) for 5 min on ice. After centrifugation at $12,000 \times g$ for 5 min, the supernatants containing the cytoplasmic fraction of RNA were collected. The pelleted nuclei were washed with lysis buffer twice and were finally centrifuged as the nuclear fraction. Cytoplasmic and nuclear RNA were then extracted by TRIzol reagent. RNA was reversed transcribed using M-MLV Reverse Transcriptase (Thermo Fisher Scientific). The reverse-transcription products from samples in the various treatment

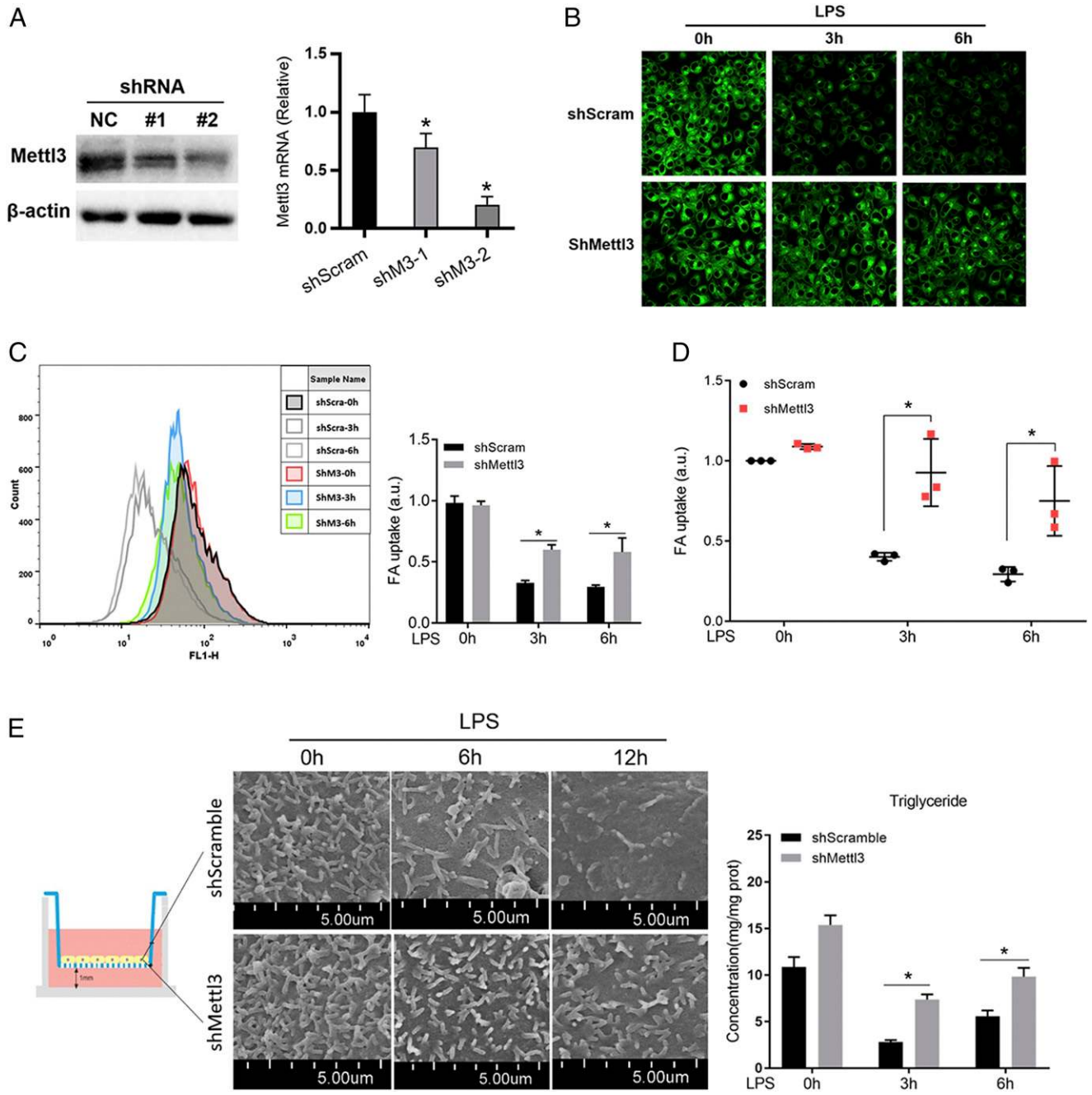


**FIGURE 2.** Mettl3 depletion prevents LPS-induced malabsorption of LCFA. (**A**) IB of protein level (left) and q-PCR analysis of mRNA level (right) to determine the knockdown effects of established Mettl3-depletion IPEC-J2 cells. q-PCR results are presented relative to those of gapdh. (**B**–**D**) Bodipy FA (green) incubated with shMettl3 and shScramble IPEC-J2 cells for 5 min at 37°C after LPS treatment for various times. Confocal microscope was used to observe the absorption level of Bodipy FA. Original magnification ×40 (B). Flow cytometer was used to analyze the absorption level of Bodipy FA. Right panel, The relative fluorescence intensity levels (C). Microplate reader was used to measure the general level of Bodipy FA absorption (D). (**E**) Cells were seeded on a 0.4-μm Transwell and cultured for 21 d to polarize with villus formation and then following with 10 μg/ml LPS treatment for 0, 6, and 12 h. Middle panel, The SEM results of villi morphology. Right panel, The triglyceride level in whole cell lysates. The data are expressed as the mean ± SEM. Statistically significant difference relative to the corresponding time point in shScramble group ($n$ = 3, biological replicates). *$p < 0.05$. shScram, cells transfected with negative control scramble shRNA; shM3, cells transfected with Mettl3 shRNA [one of two shRNA constructs (1, 2)].

conditions were used as templates for PCR using Taq DNA polymerase (Invitrogen). PCR products were electrophoresed using 1.5% agarose gels, and images were captured using the Gel Documentation System (Clinx Science Instruments, Shanghai, China). Primers for amplifying each target are listed as follows: Traf6-Fwd: 5′-TCGCAGTAGCTCCTGTACCT-3′; Traf6-Rev: 5′-AGCTCCCGGATTTGATGGTC-3′. Tbk1-Fwd: 5′-CCAAGGAGC-TACTGCAAATGTT-3′; Tbk1-Rev: 5′-CCACTGGACGAAGGAAGCTTAT-3′. Trpm3-Fwd: 5′-CCACTTGGTCAGGGATGTCA-3′; Trpm3-Rev: 5′-TACTCTGGCAGCTCATGCAA-3′. Tns3-Fwd: 5′-CCTGTTTATGCGCGGT-GATG-3′; Tns3-Rev: 5′-CGCTTTATGAAGATGCCGCC-3′. Tak1-Fwd: 5′-CTGCAACCACAGGCAACG-3′; Tak1-Rev: 5′-GGACTGGATGAC-CTACTGCTC-3′. Gapdh-Fwd: 5′-ACATCATCCCTGCTTCTACTGG-3′; Gapdh-Rev: 5′-CTCGGACGCCTGCTTCAC-3′. Rnu6-Fwd: 5′-CTCGC-TTCGGCAGCACA-3′; Rnu6-Rev: 5′-AACGCTTCACGAATTTGC-GT-3′.

### *Fluorescence in situ hybridization and confocal microscopy*

Cells were fixed in 4% paraformaldehyde for 20 min. Fluorescence in situ hybridization (FISH) was performed as previously described (23), and images were obtained with a Leica TCS SP2 confocal laser microscope

LSM 510. Probes of Traf6 transcripts with 5′-cy3 modification are as follows: 5′-GACTGGTCGAGGATTGTAAGGCGTATCG-3′

### *m$^6$A IP analysis*

This procedure followed the published m$^6$A-sequencing assay (25), but without the construction of a cDNA library. Briefly, total RNA was first isolated using TRIzol reagent followed by fragmentation using freshly prepared RNA fragmentation buffer (10 mM Tris-HCl, pH 7, 10 mM $ZnCl_2$). For this, 500 μg fragmented RNA was incubated with 5 μg anti-m$^6$A Ab in 1× IP buffer (10 mM Tris-HCl, pH 7.4, 150 mM NaCl, and 0.1% IGEPAL CA-630) for 2 h at 4°C on a rotating wheel. After washing three times with IP buffer, bound RNA was eluted using TRIzol reagent. For comparison of the change in abundance of m$^6$A, relative enrichment was first normalized to inputs then analyzed by comparison of the data from the sample immunoprecipitated with anti-m$^6$A. All samples were analyzed in triplicate for q-PCR. All primer sequences are shown in RT-PCR section.

### *Statistical analysis*

Each experiment was performed at least in triplicate. Statistical tests were performed using GraphPad Prism version 5.01 (GraphPad Software, San Diego, CA) by one-way ANOVA and post hoc analysis by Duncan test. Data are presented as mean ± SEM. An α value of $p < 0.05$ was considered statistically significant.

## Results

### *Inhibition effect of LPS on LCFA absorption parallels m$^6$A methylation*

To broadly define the pathological effect of LPS on LCFA absorption, IPEC-J2 cells were lysed and measured the composition of fatty acids by GC/MS after stimulation with LPS for different times. As shown in Fig. 1A, LPS treatment markedly lowered concentrations of LCFA after 6 h, especially fatty acids C16:0, C16:1, C18:0, and C18:1, whereas short-chain fatty acid absorption was not inhibited, in contrast to controls and as seen previously (11). Moreover, we found that LPS treatment notably increased global m$^6$A abundance in a time-dependent manner in IPEC-J2 cells detected by m$^6$A dot blot assay with poly(A)$^+$ RNA (Fig. 1B). Overall, our data indicated that LPS treatment could reduce LCFA absorption through an m$^6$A-involved mechanism. Interestingly, the expressions of m$^6$A methyltransferase (Mettl3, Mettl14) and demethylases (Fto, Alkbh5) were analyzed by q-PCR and immunoblot. Neither mRNA nor protein level of Mettl3, Mettl14, Fto, or Alkbh5 significantly differ before and after LPS treatment (Supplemental Fig. 1A, 1B).

### *Mettl3 depletion prevents LPS-induced malabsorption of LCFA*

To investigate the role of m$^6$A, we established IPEC-J2 cell lines with depleted Mettl3 (Fig. 2A), the core methyltransferase of m$^6$A (21). In control scramble cells, we observed that the absorption of Bodipy FA was markedly disturbed by LPS stimulation using confocal microscopy. However, cells with depleted Mettl3 exhibited a sustained absorption of Bodipy FA even at 6 h after LPS stimulation (Fig. 2B). As an independent validation, a similar phenomenon was found by microplate reader and flow cytometry analysis (Fig. 2C, 2D). Triglycerides in intestinal cells reflect the fatty acids absorption (9), so IPEC-J2 cells with or without Mettl3 were cultured in Transwell for 21 d to polarize with villus formation (Fig. 2E, middle), followed by LPS treatment. As expected, the levels of triglycerides were also sustained in cells with depleted Mettl3 (Fig. 2E, right). To substantiate this finding further, we conducted rescue experiments in IPEC-J2 cells with depleted Mettl3. The sustained absorption of Bodipy FA was abolished after adding back Mettl3 but not the vector (Fig. 3A, 3B).

### *Mettl3 depletion upregulates expression of fatty acid transporters in LPS-stimulated IPEC-J2 cells*

To investigate the genetic basis of the effect of Mettl3 depletion–sustained absorption of Bodipy FA, the mRNA level of lipids metabolism related genes were determined by q-PCR. As shown in Fig. 4A, in control scramble cells, LPS stimulation downregulated the expression of fatty acid-absorption-related genes, L-Fabp and Fatp4. Interestingly, Mettl3 depletion not only prevented the decrease of L-Fabp and Fatp4 gene expression, but also

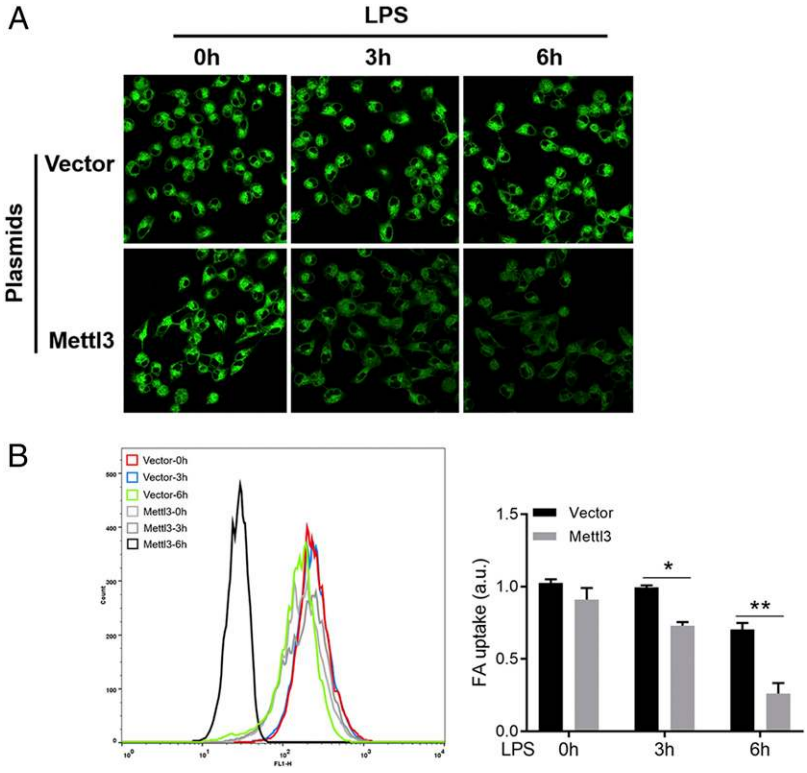


**FIGURE 3.** Adding back Mettl3 abolished the sustained absorption of Bodipy FA. Transfected Mettl3 plasmid or vector into shMettl3 IPEC-J2 cells, and then incubated with Bodipy FA (green) for 5 min at 37°C after LPS treatment for various times. Confocal microscope was used to observe the absorption level of Bodipy FA. Original magnification ×40 (**A**). Flow cytometer was used to analyze the absorption level of Bodipy FA. Right panel, The relative fluorescence intensity levels (**B**). The data are expressed as the mean ± SEM. Statistically significant difference relative to the corresponding time point in shScramble group ($n = 3$, biological replicates). *$p < 0.05$, **$p < 0.01$.

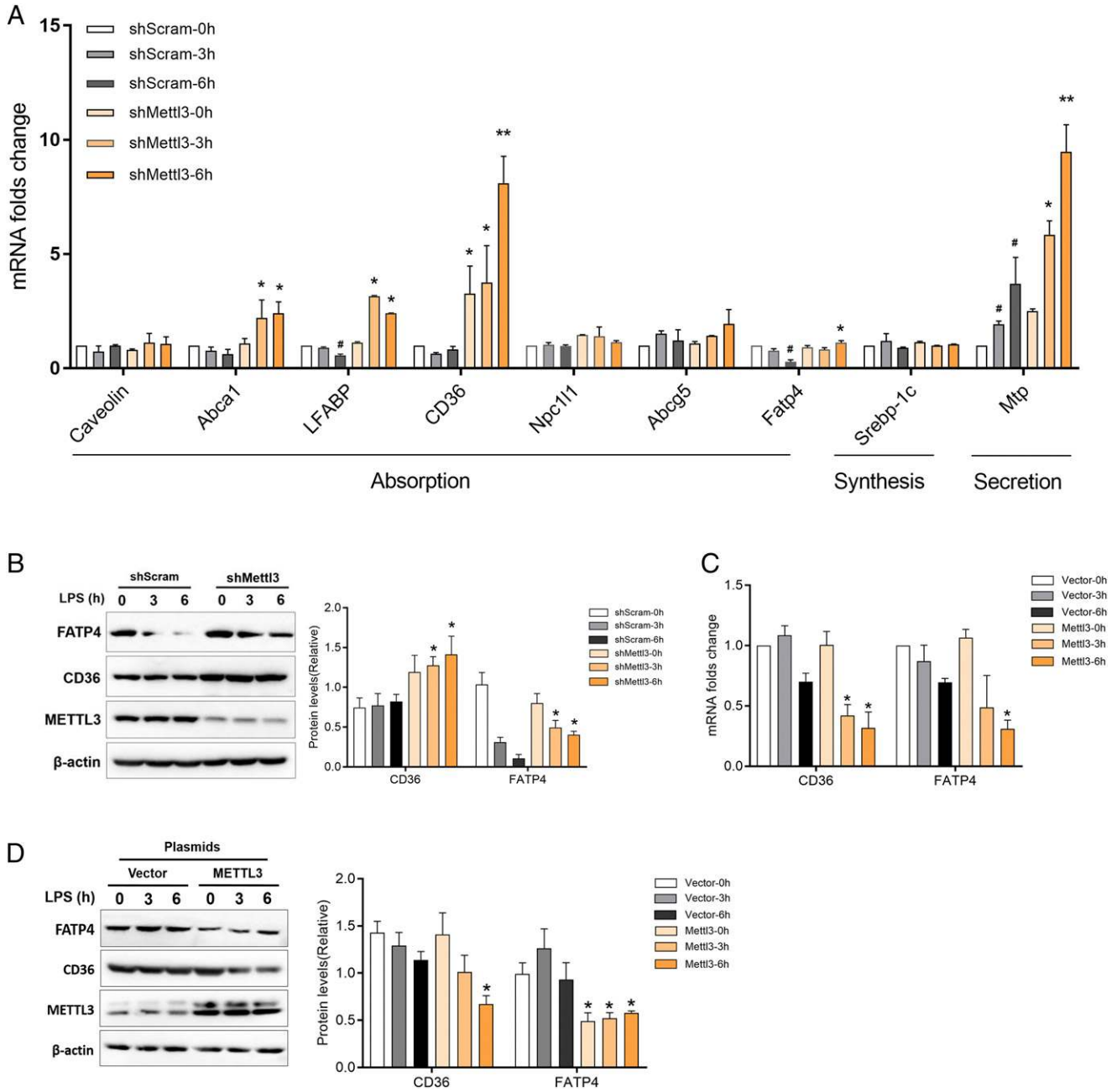


**FIGURE 4.** Mettl3 depletion upregulates expression of fatty acid transporters in LPS-stimulated IPEC-J2 cells. (**A** and **B**) shMettl3 and shScramble IPEC-J2 cells were treated with LPS for various times. q-PCR to quantify lipids metabolism related mRNA levels. *, Statistically significant difference relative to the corresponding time point in shScramble group, #, statistically significant difference relative to the 0 h in shScramble group (A). Immunoblot to determine the levels of CD36 and FATP4 (B). (**C** and **D**) q-PCR analysis of mRNA level (C) and IB of protein level (D) to determine the expression of CD36 and FATP4 in shMettl3 IPEC-J2 cells transfected in Mettl3 plasmid or vector, followed by LPS stimulation. The relative protein levels quantified by densitometry and normalized to β-actin. q-PCR results are presented relative to those of gapdh. The data are expressed as the mean ± SEM. Statistically significant difference relative to the corresponding time point in shScramble group ($n = 3$, biological replicates). $^{*}p < 0.05$ statistically significant difference relative to the corresponding time point in shScramble group, $^{**}p < 0.01$, $^{\#}p < 0.05$ statistically significant difference relative to the 0 h in shScramble group; shScram, cells transfected with negative control scramble shRNA.

upregulated the mRNA level of Abca1 and CD36, even without LPS stimulation. Thus, the previously reported important genes in fatty acid absorption, Fatp4 and CD36, were selected for further investigation (14, 15, 37–40). Similar upregulation of Fatp4 and CD36 protein expression was also observed using IB (Fig. 4B). To investigate whether Mettl3 depletion was sufficient to suppress LPS-induced Fatp4 and CD36-decreased expression further, we transfected Mettl3 plasmid into cells with depleted Mettl3 before LPS treatment. Upon LPS stimulation, the expression of Fatp4 and CD36 in cells added back with Mettl3 was decreased, compared with those in the vector-transfected cells (Fig. 4C). The decreased fatty acid transporters gene expression was accompanied with suppressed protein levels, as determined by IB (Fig. 4D). To illustrate that the effect of Mettl3 depletion is due to defective $m^6A$ modification, Alkbh5, an $m^6A$ demethylase, was depleted with siRNA (Supplemental Fig. 2A). As expected, compared with Mettl3 depletion, knocking down Alkbh5 provoked a converse decrease of CD36 and Fatp4 expression (Supplemental Fig. 2B–D).

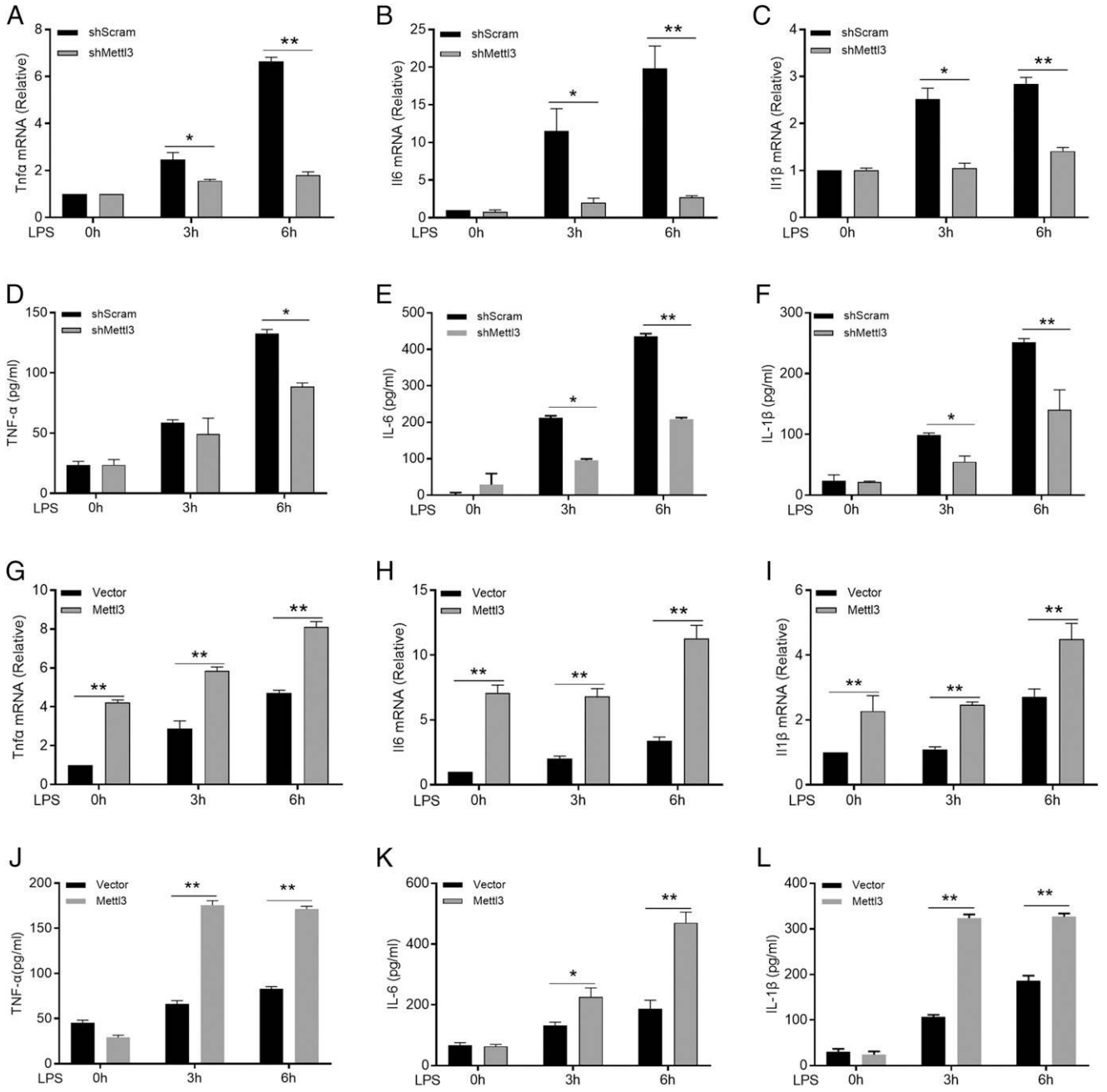


**FIGURE 5.** Mettl3 depletion prevents LPS-induced production of inflammatory cytokines. (**A**–**C**) q-PCR analysis of Tnf-α (A), Il6 (B), and Il1β (C) expression in shMettl3 and shScramble IPEC-J2 cells after LPS treatment for 0, 3, and 6 h; (**D**–**F**) ELISA analysis supernatants of the same sample as (A)–(C). (**G**–**I**) q-PCR analysis of Tnf-α (G), Il6 (H), and Il1β (I) expression in shMettl3 IPEC-J2 cells transfected in Mettl3 plasmid or vector, followed by LPS treatment. (**J**–**L**) ELISA analysis supernatants of the same sample as (G)–(I). The data are expressed as the mean ± SEM. Statistically significant difference relative to the corresponding time point in shScramble group ($n$ = 3, biological replicates). *$p < 0.05$, **$p < 0.01$. shScram, cells transfected with negative control scramble shRNA.

### *Mettl3 depletion prevents LPS-mediated production of inflammatory cytokines*

To explore the role of Mettl3 in the LPS-induced inflammatory response in IPEC-J2 cells, the expression and secretion of three typical representative inflammation cytokines (TNF-α, IL-6, and IL-1β) were determined by q-PCR and ELISA. We found that knockdown of Mettl3 led to the great decrease in both expression and secretion of TNF-α, IL-6, and IL-1β after being stimulated with LPS, compared with those in the control scramble group (Fig. 5A–F). Consistently, Mettl3 rescue experiments further confirmed that loss of Mettl3 could prevent LPS-induced expression of inflammatory cytokines in IPEC-J2 cells (Fig. 5G–I). Their protein expression levels were verified by ELISA (Fig. 5J–L). Moreover, this defective function of Mettl3 was also due to $m^6A$ modification, because a notable increase of inflammatory cytokines production was observed in cells knocking down Alkbh5 (Supplemental Fig. 3A–F).

### *Mettl3 depletion suppressed LPS-induced MAPK and NF-κB signaling pathway activation*

Due to the positive correlation between activation of MAPK and NF-κB signaling pathway and expression of inflammatory cytokines (41, 42), we sought to determine whether Mettl3 depletion affects LPS-induced NF-κB and MAPK signaling pathway activation. We found that knockdown of Mettl3 markedly suppressed

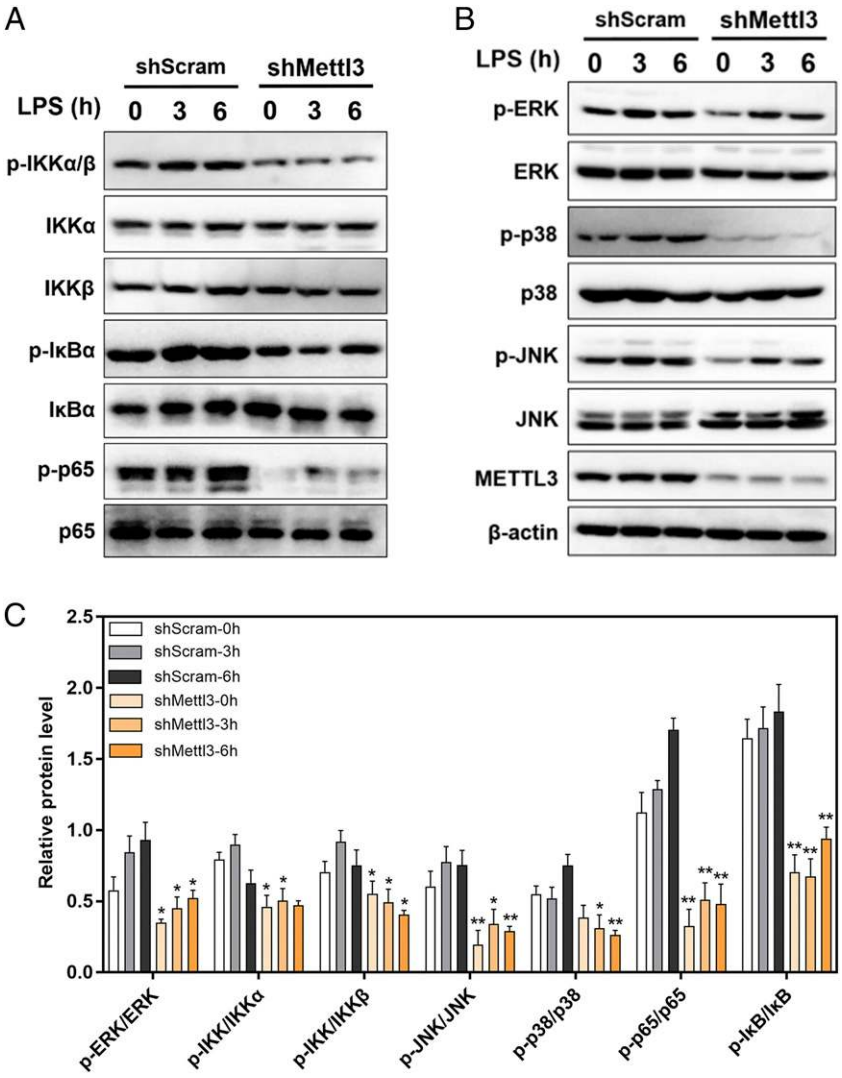


**FIGURE 6.** Mettl3 depletion suppressed LPS-induced MAPK and NF-κB signaling pathway activation. shMettl3 and shScramble IPEC-J2 cells were treated with LPS for various times. IB level of proteins in MAPK and NF-κB signaling pathway. (**A**) The phosphorylation levels of p-IKKα/β, p-p65, and p-IκBα. (**B**) The phosphorylation levels of ERK, p38, and JNK. (**C**) The relative protein levels quantified by densitometry and normalized to β-actin. The data are expressed as the mean ± SEM. Statistically significant difference relative to the control (0 h) ($n$ = 3, biological replicates). $^{*}p < 0.05$, $^{**}p < 0.01$. shScram, cells transfected with negative control scramble shRNA.

p-IKKα/β, p-p65, and p-IκBα compared with those in the control scramble group, even without LPS stimulation (Fig. 6A, 6C). Similarly, the phosphorylation levels of ERK, p38, and JNK were also reduced in the cells with depleted Mettl3 (Fig. 6B, 6C). Together, these data indicated that the suppressive effects of Mettl3 or m$^6$A modification deficiency on inflammatory cytokines production were through inactive MAPK and NF-κB signaling pathway in LPS-stimulated IPEC-J2 cells.

### *Mettl3 depletion entrapped Traf6 in the nucleus in an m$^6$A-dependent manner*

To further gain mechanistic insights into Mettl3-mediated inhibition of inflammation cytokines production in LPS-stimulated cells, we focused on TRAF6 that was upstream of both MAPK and NF-κB signaling pathway (43). As shown in Fig. 7A, compared with control scramble cells, the decreased protein levels of TRAF6 were found in Mettl3 knockdown cells before and after LPS stimulation.

As Mettl3 is a methyltransferase of m$^6$A methylation, we explored the role of m$^6$A modification in Traf6 expression. m$^6$A IP combined with q-PCR were performed with mRNA isolated from IPEC-J2 cells and found all of Traf6, Tak1, and Tns3 mRNA showed anti-m$^6$A–bound enrichment, especially Tns3, the positive control (44), relative to the abundance of these mRNAs in fractions obtained with IgG. Conversely, the anti-m$^6$A–bound enrichment was not found in the negative control (trpm3 mRNA) (30) and Tbk1 (Fig. 7B). Furthermore, to ascertain whether Traf6 transcript is a substrate for Mettl3, we determined the Traf6 m$^6$A methylation levels following Mettl3 or Alkbh5 knockdown. The decreased enrichment for Traf6 and Tak1, but not trpm3 and Tbk1, was detected when Mettl3 was knocked down, but increased enrichment was observed when Alkbh5 was knocked down (Fig. 7C). Together, our data indicate that Mettl3 mainly affects Traf6 expression through its methylation activity.

Erasure of the m$^6$A modification of mRNAs can induce retention of the mRNAs in the nucleus (28, 30). q-PCR and RT-PCR were performed with nucleocytoplasmic fractionations of RNA; we found that loss of Mettl3 increased the level of Traf6 transcripts in the nucleus but decreased its level in the cytoplasm, especially after LPS stimulation (Fig. 7D–F). FISH analysis also further confirmed that knockdown of Mettl3 increased the retention of Traf6 mRNA in the nucleus with or without LPS stimulation, in contrast to the control scramble group (Fig. 7F). Collectively, our data demonstrate that Traf6 is a direct target of Mettl3 and will be entrapped in the nucleus when Mettl3 is knocked down.

### *TRAF6 reinstates LPS-induced malabsorption of LCFA in Mettl3-depletion IPEC-J2 cells*

To ascertain whether TRAF6 is a major contributor to the function of Mettl3 in fatty acid absorption, we assessed whether adding back TRAF6 could reverse the effects of Mettl3 inhibition. Forced expression of the Traf6 significantly reduced the expression of

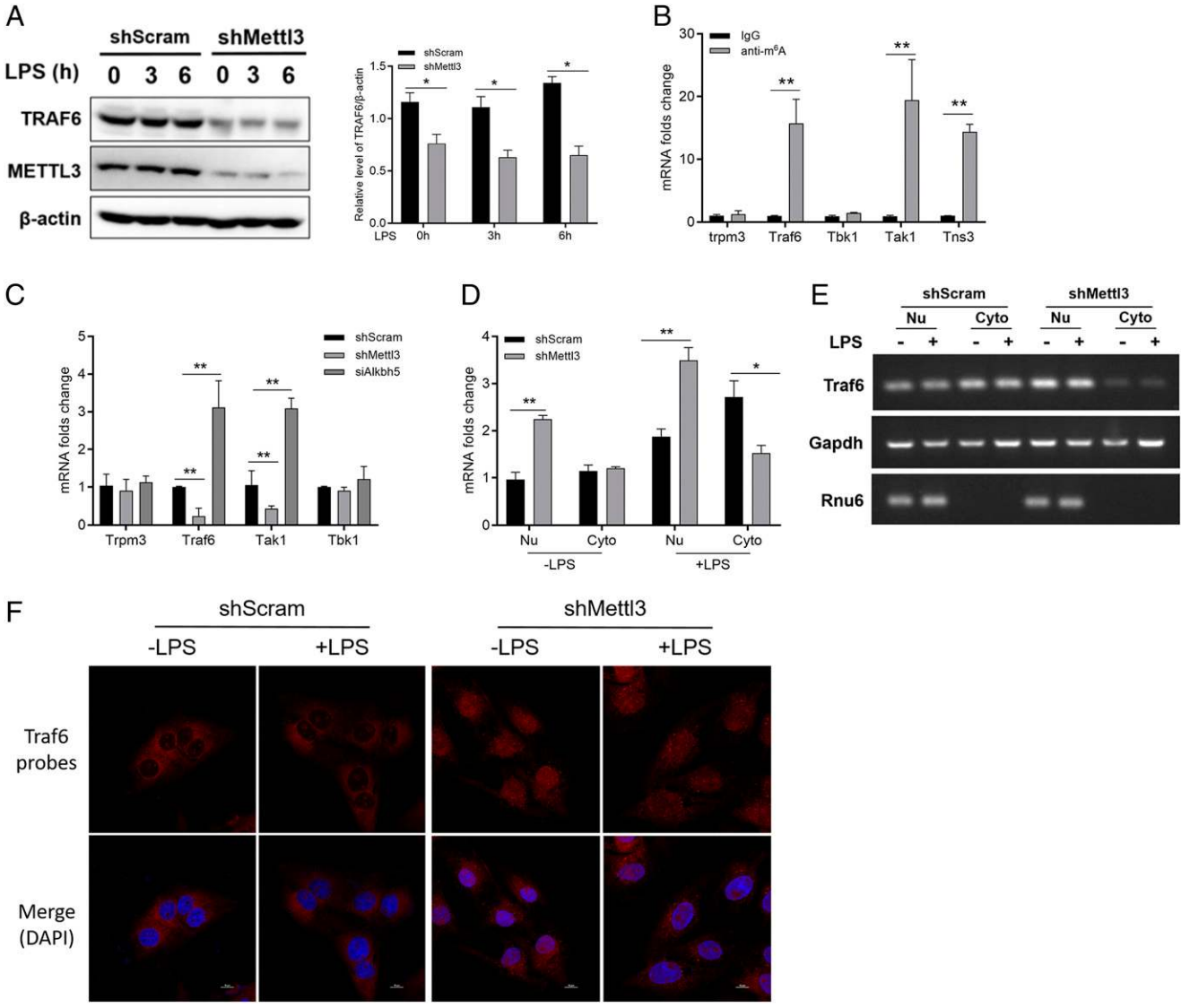


**FIGURE 7.** Mettl3 depletion entrapped Traf6 in the nucleus in an m$^6$A dependent manner. (**A**) The protein level of TRAF6 in shMettl3 or shScramble IPEC-J2 cells was determined by immunoblot. The right panel shows the relative protein levels quantified by densitometry and normalized to β-actin. (**B** and **C**) m$^6$A IP combined with q-PCR analysis with mRNA isolated from wild IPEC-J2 cells (B), shScramble, shMettl3, and siAlkbh5 IPEC-J2 cells (C). (**D** and **E**) q-PCR (D) and RT-PCR (E) analysis the distribution of Traf6 mRNA in the nucleus or cytoplasm in shMettl3 and shScramble cells with or without LPS stimulation. (**F**) FISH analysis of Traf6 transcripts in shMettl3 and shScramble cells treated as in (D). Scale bars, 5 μm. The data are expressed as the mean ± SEM. Statistically significant difference relative to the corresponding time point in shScram group ($n$ = 3, biological replicates). *$p < 0.05$, **$p < 0.01$. shScram, cells transfected with negative control scramble shRNA.

Fatp4 and CD36 at both protein and mRNA levels in Mettl3-depletion IPEC-J2 cells, compared with the vector-transfected cells (Fig. 8A, 8B). Furthermore, ectopic expression of Traf6 largely abolished sustained absorption of Bodipy FA in Mettl3 depletion cells. The phenomenon was observed using confocal microscopy and flow cytometry (Fig. 8C, 8D). These results suggest that Mettl3 and Traf6 cooperate in the regulation of fatty acid transporters expression and play important roles in LCFA absorption.

## Discussion

We aimed to elucidate the mechanisms of malabsorption of LCFA during the pathological processes. In this study, we provide compelling evidence demonstrating that loss of Mettl3 could sustain the absorption of LCFA in the inflammation process through entrapping the Traf6 in the nucleus.

Consistent with a previous study (11), we found LPS treatment could severely reduce the absorption of LCFA, whereas short-chain fatty acid absorption was not inhibited. Unexpectedly, the reduced LCFA absorption was accompanied with a marked increase of m$^6$A modification levels, whereas Mettl3, Mettl14, Fto, and Alkbh5 expression levels did not significantly differ with or without LPS stimulation. At first glance, our data would appear to conflict with the previous study, whose expression increased after LPS stimulation in dental pulp cells (29). Indeed, similar with several RNA processing factors including ASF/SF2, hnRNPA1, HuR, and TDP-43 (45, 46), subcellular distribution of m$^6$A methyltransferases showed alteration in response to different cell stress stimuli (47). However, further study of the detailed mechanism of m$^6$A methyltransferases' action on m$^6$A modification in inflammation response is warranted. Nevertheless, these findings indicated that m$^6$A modification might be involved in the LPS-induced malabsorption of LCFA.

Mettl3 was originally identified as a methyltransferase responsible for m$^6$A modification in mRNA (48). Mettl3 knockdown in

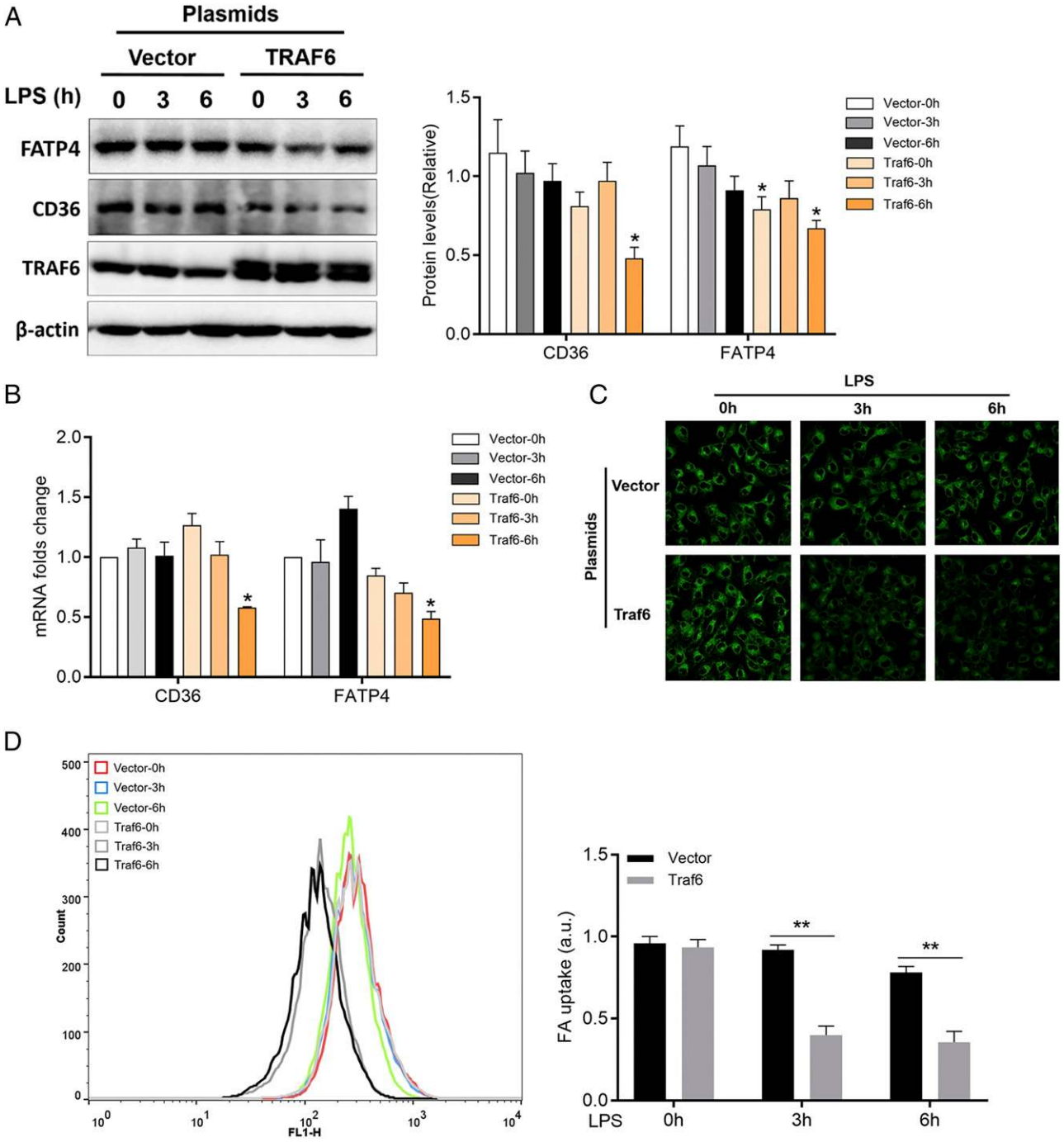


**FIGURE 8.** TRAF6 reinstates LPS-induced malabsorption of LCFA in Mettl3 depletion IPEC-J2 cells. (**A** and **B**) Transfected Traf6 plasmid or vector into shMettl3 IPEC-J2 cells, followed by LPS stimulation for various time. IB of protein level (A) and q-PCR analysis of mRNA level (B) to determine the expression of CD36 and FATP4. (**C** and **D**) Ectopic expression of Traf6 abolished sustained absorption of Bodipy FA in Mettl3 depletion cells. Confocal microscope was used to observe the absorption level of Bodipy FA. Original magnification ×40 (C). Flow cytometer was used to analyze the absorption level of Bodipy FA. Right panel, The relative fluorescence intensity levels (D). The relative protein levels quantified by densitometry and normalized to β-actin. q-PCR results are presented relative to those of gapdh. The data are expressed as the mean ± SEM. Statistically significant difference relative to the corresponding time point in shScramble group ($n$ = 3, biological replicates). *$p < 0.05$, **$p < 0.01$.

murine embryonic stem cells and Hela cells result in reduced $m^6A$ abundance (49, 50). To investigate the role of $m^6A$, we established IPEC-J2 cell lines with depleted Mettl3. The data show the compelling fact that cells with depleted Mettl3 exhibited a sustained absorption of Bodipy FA after LPS stimulation. Moreover, we found Mettl3 depletion upregulated expression of fatty acid transporters, compared with those in shScramble IPEC-J2 cells. Interestingly, Mettl3 depletion exhibited the regulation effects of some fatty acid transporters even without LPS stimulation, such as Abca1 and CD36. Theoretically, there were three probable molecular mechanisms for the expression of fatty acid transporters in Mettl3 knockdown cells after LPS stimulation: 1) depletion of Mettl3 suppressed the response triggered by LPS, 2) depletion of Mettl3 directly activated the signaling pathway of fatty acid transporters expression, or 3) both. In this study, we explored the possibility that deficiency of Mettl3 blocks the effects of LPS.

Nevertheless, at the moment we cannot exclude the possibility that loss of Mettl3 also targets the fatty acid transporters expression signaling pathway directly. Moreover, we believe that the effect of Mettl3 depletion on fatty acid transporters expression was due to defective $m^6A$ modification, because the converse results were observed in Alkbh5 ($m^6A$ demethylase) knockdown cells.

Previous studies revealed that LPS stimulation could induce the intestinal inflammation in IPEC-J2 cells (51). Therefore, production of inflammatory cytokines was determined to address the hypothesis that Mettl3 sustained absorption of Bodipy FA in LPS-stimulated cells through blocking the inflammation response. The results confirmed our hypothesis and were consistent with a previous study on LPS activation on dental pulp cells, which furtherly found $m^6A$ modification is necessary to generate a dominant negative version of MyD88 that presumably may mediate signaling blockade (29). Furthermore, we found both NF-κB and MAPK signaling pathways were suppressed in Mettl3 depletion cells after LPS stimulation. However, $m^6A$ methylation did not affect the activity of the cytokines expression induced by the adaptor MyD88 (30). These data suggested that $m^6A$ functioned downstream of MyD88 and upstream of NF-κB and MAPK. Expectedly, the markedly decreased protein level of TRAF6 were observed in Mettl3 knockdown cells before and after LPS stimulation. Further supporting this notion, $m^6A$ IP data demonstrated that Traf6 mRNA was a direct target of Mettl3, because deficiency of Mettl3 decreased the abundance of Traf6 mRNA.

The retention of mRNA in the nucleus mediated by NFs plays an important role in the regulation of gene expression (52). Erasure of the $m^6A$ modification of mRNAs can induce retention of the mRNAs in the nucleus (28, 30). We also found that Mettl3 depletion was able to entrap Traf6 transcripts in the nucleus after LPS stimulation. However, the fate of the entrapped Traf6 transcripts needs to be investigated further. A previously study revealed that mature mRNAs, mRNAs retained in the nucleus, and pre-mRNAs could be degraded (53), so we speculated that the entrapped Traf6 induced by Mettl3 depletion were degraded. These results inspired us to hypothesize that Mettl3 sustained the absorption of LCFA by entrapping Traf6 transcripts in nucleus to suppress the inflammation response. Consistently, forced expression of Traf6 largely abolished sustained absorption of fatty acids in Mettl3-depleted cells.

Overall, we clarify the relationship between inflammation and fatty acids absorption. Mechanistically, we reported that depletion of Mettl3 could decrease the $m^6A$ level of Traf6, resulting in its transcripts being retained in the nucleus, followed by inactivation of NF-κB and MAPK signaling pathways. Thus, the inflammation response was suppressed, leading to the absorption of LCFA being sustained. The insights obtained from this study further advance our understanding of the mechanisms of LPS-mediated malabsorption and provide novel approaches to the treatment and the prevention of fatty acid–related metabolic diseases.

## Acknowledgments

We thank Wang laboratory members for helpful discussion.

## Disclosures

The authors have no financial conflicts of interest.

## References

1. Makrides, M., C. T. Collins, and R. A. Gibson. 2011. Impact of fatty acid status on growth and neurobehavioural development in humans. *Matern. Child Nutr.* 7 (Suppl. 2): 80–88.
2. Wang, D. Q. H. 2007. Regulation of intestinal cholesterol absorption. *Annu. Rev. Physiol.* 69: 221–248.
3. Lammert, F., and D. Q. H. Wang. 2005. New insights into the genetic regulation of intestinal cholesterol absorption. *Gastroenterology* 129: 718–734.
4. Schwenk, R. W., G. P. Holloway, J. J. F. P. Luiken, A. Bonen, and J. F. C. Glatz. 2010. Fatty acid transport across the cell membrane: regulation by fatty acid transporters. *Prostaglandins Leukot. Essent. Fatty Acids* 82: 149–154.
5. Abumrad, N., C. Harmon, and A. Ibrahimi. 1998. Membrane transport of long-chain fatty acids: evidence for a facilitated process. *J. Lipid Res.* 39: 2309–2318.
6. Stahl, A., D. J. Hirsch, R. E. Gimeno, S. Punreddy, P. Ge, N. Watson, S. Patel, M. Kotler, A. Raimondi, L. A. Tartaglia, and H. F. Lodish. 1999. Identification of the major intestinal fatty acid transport protein. *Mol. Cell* 4: 299–308.
7. Poirier, H., P. Degrace, I. Niot, A. Bernard, and P. Besnard. 1996. Localization and regulation of the putative membrane fatty-acid transporter (FAT) in the small intestine. Comparison with fatty acid-binding proteins (FABP). *Eur. J. Biochem.* 238: 368–373.
8. Zilversmit, D. B. 1965. The composition and structure of lymph chylomicrons in dog, rat, and man. *J. Clin. Invest.* 44: 1610–1622.
9. Redgrave, T. G., and K. B. Dunne. 1975. Chylomicron formation and composition in unanaesthetised rabbits. *Atherosclerosis* 22: 389–400.
10. Fijlstra, M., W. J. E. Tissing, F. Stellaard, H. J. Verkade, and E. H. H. M. Rings. 2013. Reduced absorption of long-chain fatty acids during methotrexate-induced gastrointestinal mucositis in the rat. *Clin. Nutr.* 32: 452–459.
11. Yoshioka, M., H. Asakura, S. Miura, Y. Hamada, K. Kobayashi, T. Morishita, A. Morita, and M. Tsuchiya. 1986. Malabsorption of long-chain fatty acid in cholera toxin-induced secretory diarrhea. *Dig. Dis. Sci.* 31: 519–523.
12. Chung, K. W., K. M. Kim, Y. J. Choi, H. J. An, B. Lee, D. H. Kim, E. K. Lee, E. Im, J. Lee, D. S. Im, et al. 2017. The critical role played by endotoxin-induced liver autophagy in the maintenance of lipid metabolism during sepsis. *Autophagy* 13: 1113–1129.
13. Mao, K., A. P. Baptista, S. Tamoutounour, L. Zhuang, N. Bouladoux, A. J. Martins, Y. Huang, M. Y. Gerner, Y. Belkaid, and R. N. Germain. 2018. Innate and adaptive lymphocytes sequentially shape the gut microbiota and lipid metabolism. *Nature* 554: 255–259.
14. Glatz, J. F. C., and J. J. F. P. Luiken. 2018. Dynamic role of the transmembrane glycoprotein CD36 (SR-B2) in cellular fatty acid uptake and utilization. *J. Lipid Res.* 59: 1084–1093.
15. Gajda, A. M., and J. Storch. 2015. Enterocyte fatty acid-binding proteins (FABPs): different functions of liver and intestinal FABPs in the intestine. *Prostaglandins Leukot. Essent. Fatty Acids* 93: 9–16.
16. Baranova, I. N., T. G. Vishnyakova, A. V. Bocharov, A. Leelahavanichkul, R. Kurlander, Z. Chen, A. C. P. Souza, P. S. T. Yuen, R. A. Star, G. Csako, et al. 2012. Class B scavenger receptor types I and II and CD36 mediate bacterial recognition and proinflammatory signaling induced by *Escherichia coli*, lipopolysaccharide, and cytosolic chaperonin 60. *J. Immunol.* 188: 1371–1380.
17. Baranova, I. N., R. Kurlander, A. V. Bocharov, T. G. Vishnyakova, Z. Chen, A. T. Remaley, G. Csako, A. P. Patterson, and T. L. Eggerman. 2008. Role of human CD36 in bacterial recognition, phagocytosis, and pathogen-induced JNK-mediated signaling. *J. Immunol.* 181: 7147–7156.
18. Hoebe, K., P. Georgel, S. Rutschmann, X. Du, S. Mudd, K. Crozat, S. Sovath, L. Shamel, T. Hartung, U. Zähringer, and B. Beutler. 2005. CD36 is a sensor of diacylglycerides. *Nature* 433: 523–527.
19. Cifarelli, V., S. Ivanov, Y. Xie, N. H. Son, B. T. Saunders, T. A. Pietka, T. M. Shew, J. Yoshino, S. Sundaresan, N. O. Davidson, et al. 2017. CD36 deficiency impairs the small intestinal barrier and induces subclinical inflammation in mice. *Cell. Mol. Gastroenterol. Hepatol.* 3: 82–98.
20. Fischer, J., L. Koch, C. Emmerling, J. Vierkotten, T. Peters, J. C. Brüning, and U. Rüther. 2009. Inactivation of the Fto gene protects from obesity. *Nature* 458: 894–898.
21. Liu, J., Y. Yue, D. Han, X. Wang, Y. Fu, L. Zhang, G. Jia, M. Yu, Z. Lu, X. Deng, et al. 2014. A METTL3-METTL14 complex mediates mammalian nuclear RNA N6-adenosine methylation. *Nat. Chem. Biol.* 10: 93–95.
22. Jia, G., Y. Fu, X. Zhao, Q. Dai, G. Zheng, Y. Yang, C. Yi, T. Lindahl, T. Pan, Y. G. Yang, and C. He. 2011. N6-methyladenosine in nuclear RNA is a major substrate of the obesity-associated FTO. [Published erratum appears in 2012 *Nat. Chem. Biol.* 8: 1008.] *Nat. Chem. Biol.* 7: 885–887.
23. Wang, X., Z. Lu, A. Gomez, G. C. Hon, Y. Yue, D. Han, Y. Fu, M. Parisien, Q. Dai, G. Jia, et al. 2014. N6-methyladenosine-dependent regulation of messenger RNA stability. *Nature* 505: 117–120.
24. Zheng, G., J. A. Dahl, Y. Niu, P. Fedorcsak, C. M. Huang, C. J. Li, C. B. Vågbø, Y. Shi, W. L. Wang, S. H. Song, et al. 2013. ALKBH5 is a mammalian RNA demethylase that impacts RNA metabolism and mouse fertility. *Mol. Cell* 49: 18–29.
25. Zhao, X., Y. Yang, B. F. Sun, Y. Shi, X. Yang, W. Xiao, Y. J. Hao, X. L. Ping, Y. S. Chen, W. J. Wang, et al. 2014. FTO-dependent demethylation of N6-methyladenosine regulates mRNA splicing and is required for adipogenesis. *Cell Res.* 24: 1403–1419.
26. Barbieri, I., K. Tzelepis, L. Pandolfini, J. Shi, G. Millán-Zambrano, S. C. Robson, D. Aspris, V. Migliori, A. J. Bannister, N. Han, et al. 2017. Promoter-bound METTL3 maintains myeloid leukaemia by $m^6A$-dependent translation control. *Nature* 552: 126–131.
27. Geula, S., S. Moshitch-Moshkovitz, D. Dominissini, A. A. Mansour, N. Kol, M. Salmon-Divon, V. Hershkovitz, E. Peer, N. Mor, Y. S. Manor, et al. 2015. Stem cells. m6A mRNA methylation facilitates resolution of naïve pluripotency toward differentiation. *Science* 347: 1002–1006.
28. Fustin, J. M., M. Doi, Y. Yamaguchi, H. Hida, S. Nishimura, M. Yoshida, T. Isagawa, M. S. Morioka, H. Kakeya, I. Manabe, and H. Okamura. 2013. RNA-methylation-dependent RNA processing controls the speed of the circadian clock. *Cell* 155: 793–806.

29. Feng, Z., Q. Li, R. Meng, B. Yi, and Q. Xu. 2018. METTL3 regulates alternative splicing of MyD88 upon the lipopolysaccharide-induced inflammatory response in human dental pulp cells. *J. Cell. Mol. Med.* 22: 2558–2568.
30. Zheng, Q., J. Hou, Y. Zhou, Z. Li, and X. Cao. 2017. The RNA helicase DDX46 inhibits innate immunity by entrapping $m^6A$-demethylated antiviral transcripts in the nucleus. *Nat. Immunol.* 18: 1094–1103.
31. Zong, X., D. Song, T. Wang, X. Xia, W. Hu, F. Han, and Y. Wang. 2015. LFP-20, a porcine lactoferrin peptide, ameliorates LPS-induced inflammation via the MyD88/NF-κB and MyD88/MAPK signaling pathways. *Dev. Comp. Immunol.* 52: 123–131.
32. Zhou, J., J. Wan, X. E. Shu, Y. Mao, X. M. Liu, X. Yuan, X. Zhang, M. E. Hess, J. C. Brüning, and S. B. Qian. 2018. $N^6$-Methyladenosine guides mRNA alternative translation during integrated stress response. *Mol. Cell* 69: 636–647.e7.
33. Chen, H. K., S. N. Song, L. H. Wang, A. B. Mayfield, Y. J. Chen, W. N. Chen, and C. S. Chen. 2015. A compartmental comparison of major lipid species in a coral-symbiodinium endosymbiosis: evidence that the coral host regulates lipogenesis of its cytosolic lipid bodies. *PLoS One* 10: e0132519.
34. Jang, C., S. F. Oh, S. Wada, G. C. Rowe, L. Liu, M. C. Chan, J. Rhee, A. Hoshino, B. Kim, A. Ibrahim, et al. 2016. A branched-chain amino acid metabolite drives vascular fatty acid transport and causes insulin resistance. *Nat. Med.* 22: 421–426.
35. Stremmel, W., S. Staffer, A. Wannhoff, and A. Pathil. 2017. The overall fatty acid absorption controlled by basolateral chylomicron excretion under regulation of p-JNK1. Biochim. Biophys. Acta Mol. Cell Biol Lipids 1862: 917–928.
36. Mayer, A., and L. S. Churchman. 2016. Genome-wide profiling of RNA polymerase transcription at nucleotide resolution in human cells with native elongating transcript sequencing. *Nat. Protoc.* 11: 813–833.
37. Esteves, A., A. Knoll-Gellida, L. Canclini, M. C. Silvarrey, M. André, and P. J. Babin. 2016. Fatty acid binding proteins have the potential to channel dietary fatty acids into enterocyte nuclei. *J. Lipid Res.* 57: 219–232.
38. Trevaskis, N. L., G. Nguyen, M. J. Scanlon, and C. J. Porter. 2011. Fatty acid binding proteins: potential chaperones of cytosolic drug transport in the enterocyte? *Pharm. Res.* 28: 2176–2190.
39. Nauli, A. M., F. Nassir, S. Zheng, Q. Yang, C. M. Lo, S. B. Vonlehmden, D. Lee, R. J. Jandacek, N. A. Abumrad, and P. Tso. 2006. CD36 is important for chylomicron formation and secretion and may mediate cholesterol uptake in the proximal intestine. *Gastroenterology* 131: 1197–1207.
40. Drover, V. A., M. Ajmal, F. Nassir, N. O. Davidson, A. M. Nauli, D. Sahoo, P. Tso, and N. A. Abumrad. 2005. CD36 deficiency impairs intestinal lipid secretion and clearance of chylomicrons from the blood. *J. Clin. Invest.* 115: 1290–1297.
41. Wei, Z. F., B. Tong, Y. F. Xia, Q. Lu, G. X. Chou, Z. T. Wang, and Y. Dai. 2013. Norisoboldine suppresses osteoclast differentiation through preventing the accumulation of TRAF6-TAK1 complexes and activation of MAPKs/NF-κB/c-Fos/NFATc1 pathways. *PLoS One* 8: e59171.
42. Chen, L. F., and W. C. Greene. 2004. Shaping the nuclear action of NF-kappaB. *Nat. Rev. Mol. Cell Biol.* 5: 392–401.
43. Liu, J., and X. Cao. 2016. Cellular and molecular regulation of innate inflammatory responses. *Cell. Mol. Immunol.* 13: 711–721.
44. Dominissini, D., S. Moshitch-Moshkovitz, S. Schwartz, M. Salmon-Divon, L. Ungar, S. Osenberg, K. Cesarkas, J. Jacob-Hirsch, N. Amariglio, M. Kupiec, et al. 2012. Topology of the human and mouse m6A RNA methylomes revealed by m6A-seq. *Nature* 485: 201–206.
45. Biamonti, G., and J. F. Caceres. 2009. Cellular stress and RNA splicing. *Trends Biochem. Sci.* 34: 146–153.
46. Zhang, T., G. Baldie, G. Periz, and J. Wang. 2014. RNA-processing protein TDP-43 regulates FOXO-dependent protein quality control in stress response. *PLoS Genet.* 10: e1004693.
47. Wen, J., R. Lv, H. Ma, H. Shen, C. He, J. Wang, F. Jiao, H. Liu, P. Yang, L. Tan, et al. 2018. Zc3h13 regulates nuclear RNA $m^6A$ methylation and mouse embryonic stem cell self-renewal. *Mol. Cell* 69: 1028–1038.e6.
48. Bokar, J. A., M. E. Shambaugh, D. Polayes, A. G. Matera, and F. M. Rottman. 1997. Purification and cDNA cloning of the AdoMet-binding subunit of the human mRNA (N6-adenosine)-methyltransferase. *RNA* 3: 1233–1247.
49. Wang, Y., Y. Li, J. I. Toth, M. D. Petroski, Z. Zhang, and J. C. Zhao. 2014. N6-methyladenosine modification destabilizes developmental regulators in embryonic stem cells. *Nat. Cell Biol.* 16: 191–198.
50. Yue, Y., J. Liu, and C. He. 2015. RNA N6-methyladenosine methylation in post-transcriptional gene expression regulation. *Genes Dev.* 29: 1343–1355.
51. Zong, X., W. Hu, D. Song, Z. Li, H. Du, Z. Lu, and Y. Wang. 2016. Porcine lactoferrin-derived peptide LFP-20 protects intestinal barrier by maintaining tight junction complex and modulating inflammatory response. *Biochem. Pharmacol.* 104: 74–82.
52. Sun, X., P. P. Li, S. Zhu, R. Cohen, L. O. Marque, C. A. Ross, S. M. Pulst, H. Y. Chan, R. L. Margolis, and D. D. Rudnicki. 2015. Nuclear retention of full-length HTT RNA is mediated by splicing factors MBNL1 and U2AF65. *Sci. Rep.* 5: 12521.
53. Kufel, J., C. Bousquet-Antonelli, J. D. Beggs, and D. Tollervey. 2004. Nuclear pre-mRNA decapping and 5′ degradation in yeast require the Lsm2-8p complex. *Mol. Cell. Biol.* 24: 9646–9657.